Multitransient electromagnetic demonstration survey in France

GEOPHYSICS, VOL. 72, NO. 4 (JULY-AUGUST 2007); P. F197–F209, 20 FIGS., 2 TABLES.
10.1190/1.2735802

Multitransient electromagnetic demonstration survey in France

Anton Ziolkowski[1], Bruce A. Hobbs[1], and David Wright[1]

ABSTRACT

We describe the acquisition, processing, and inversion of a multitransient electromagnetic (MTEM) single-line survey, conducted in December 2004 over an underground gas storage reservoir in southwestern France. The objective was to find a resistor corresponding to known gas about 500 m below the survey line. In data acquisition, we deployed a 100-m inline bipole current source and twenty 100-m inline potential receivers in various configurations along the 5-km survey line; we measured the input current step and received voltages simultaneously. Then we deconvolved the received voltages for the measured input current to determine the earth impulse responses. We show how both amplitude and traveltime information contained in the recovered earth impulse responses reveal the lateral location and approximate depth of the resistive reservoir. Integrating the impulse responses yields step responses, from which the asymptotic DC values were estimated and used in rapid 2D dipole-dipole DC resistivity inversion to find the top of the reservoir. A series of collated 1D full-waveform inversions performed on individual common midpoint gathers of the step responses position the top and bottom of a resistor corresponding to known gas in the reservoir and also obtain the transverse resistance. The results imply that the MTEM method can be used as a tool for hydrocarbon exploration and production.

INTRODUCTION

Porous rocks are saturated with fluids. The fluids may be water, gas, oil, or a mixture of all three. The flow of electric current in the earth is determined by the resistivities of such rocks, which are affected by the saturating fluids. For instance, brine-saturated porous rocks are much less resistive than the same rocks filled with hydrocarbons (e.g., Archie, 1942). Hence, the exploration objective is to determine whether hydrocarbons are present by measuring the resistivity of geologic formations. If tests using other methods, e.g., seismic exploration, suggest that a geologic formation has the potential to bear hydrocarbons, then, before drilling, it is important to have some indication of whether the formation contains hydrocarbons or whether it is primarily water bearing. This can be done using electromagnetic (EM) techniques and, more specifically, time-domain EM techniques.

Kaufman and Keller (1983) give the theoretical basis for the use of transient EM methods and show that resistive layers can be resolved best by measuring the electric fields from a galvanic source. Rocroi and Gole (1983) describe the use of grounded dipole current sources on a transmission axis and dipole receivers on a parallel receiver axis. They apply transient boxcar pulses at the sources and analyze the signal at the receiver from the time the source current is switched off, i.e., they aim to measure the step response of the earth. Strack et al. (1989) describe the long-offset transient electromagnetic (LOTEM) method, including the data interpretation. LOTEM uses a 1–2 km grounded bipole current source 5–20 km from an array of EM receivers: horizontal magnetic loops and horizontal electric bipoles. The source-current waveform is a square wave, alternating between positive and negative polarity. The received response is a series of step responses of alternating polarity. In the interpretation of the data, Strack et al. (1989) use 1D inversion and place the resulting earth model beneath the receiver. Strack (1992) contains three chapters on case histories of LOTEM exploration and, in each case, the 1D inversion results are posted vertically beneath the receivers. The reciprocity principle states that the impulse response of the earth for a dipole-dipole configuration is the same when source at A and receiver at B are interchanged, so the inversion would give the same result in both situations, but in one case the result would be posted at A and in the other at B. It makes more sense to post the 1D inversion result at the midpoint between source and receiver: The result is invariant when source and receiver are interchanged.

The multitransient electromagnetic (MTEM) method differs from previous transient EM work in that both the received voltage and the input current are measured simultaneously, and the impulse response of the earth is recovered from these two measurements by deconvolution. This is new. A patent application was filed in 2001 and granted in the United States in 2005 (Wright et al., 2005). Recovering the impulse response allows the data to be processed in a manner

Manuscript received by the Editor August 11, 2006; revised manuscript received February 16, 2007; published online May 25, 2007.
[1]MTEM Limited, Edinburgh, United Kingdom. E-mail: anton.ziolkowski@mtem.com; bruce.hobbs@mtem.com; david.wright@mtem.com.

similar to seismic data processing, and this has allowed us to make significant progress. We use seismic data-processing software for data handling, processing, and display.

Wright et al. (2002) describe an MTEM survey over an underground gas storage reservoir near Paris. Inline and crossline bipole current sources and inline and crossline electric-field bipole receivers were laid out along a line; horizontal magnetic loops also were used to measure the vertical component of the rate of change of the magnetic field. Wright (2003) analyzes all the data from this survey and finds that only the inline source and inline receivers need be used. The other components provided no additional information. Wright et al. (2002) use only the inline source and inline receiver data. They recover the time derivative of the earth-impulse responses by deconvolution and differentiation and display them as common-offset sections, with the source-receiver midpoint as the horizontal coordinate and time as the vertical axis. This clearly shows the resistor corresponding to the known gas in the correct lateral position. Note that common-offset sections are standard displays in seismic data processing.

Here, we describe an MTEM survey over an underground gas storage reservoir in southwestern France, conducted in December 2004. The survey was part of a collaborative project between the multinational oil company TOTAL, MTEM Ltd., and the University of Edinburgh to test the MTEM method's ability to detect resistive hydrocarbons. It followed from an earlier survey, conducted in January 2004, which was part of a Scottish Enterprise Proof of Concept Project.The primary objective of the survey was to locate the gas-bearing part of the reservoir. A secondary objective was to determine its thickness and resistivity.

We outline the MTEM method, using 1D modeling to illustrate the salient points, and then describe the field procedure, equipment, and field parameters. We describe our data-processing procedure, with emphasis on the use of the reciprocity principle to check the recovered impulse responses.We show that the processed data can be interpreted in four different ways to estimate subsurface resistivities. The results of these four approaches are consistent with each other and with seismic data.

THE MTEM METHOD

The MTEM method is described by Wright et al. (2001, 2002, 2005). The setup is shown in Figure 1. A time-varying current, typically a step function or a pseudo-random binary sequence (PRBS), is injected between the two source electrodes A and B and is measured and recorded. This is the input to the earth. The time-varying voltage response between the two receiver electrodes C and D is also measured simultaneously. If the response reaches steady state before the next change in current is applied at the source, the full response has been measured and is the convolution

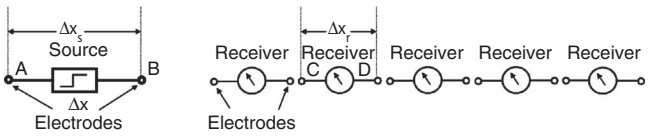

Figure 1. Plan view of a typical land MTEM source-receiver configuration with a current bipole source and its two electrodes, A and B, and a line of receivers in line with the source, measuring the potential between pairs of receiver electrodes, for instance, C and D.

$$v(k,\mathbf{x}_C,\mathbf{x}_D;\mathbf{x}_A,\mathbf{x}_B,t) = i(k,\mathbf{x}_A,\mathbf{x}_B,t)^* g(\mathbf{x}_C,\mathbf{x}_D;\mathbf{x}_A,\mathbf{x}_B,t)^* r_{CD}(t) + n(k,\mathbf{x}_C,\mathbf{x}_D,t), \quad (1)$$

in which $v(k,\mathbf{x}_C,\mathbf{x}_D;\mathbf{x}_A,\mathbf{x}_B,t)$ is the measured voltage response, $i(k,\mathbf{x}_A,\mathbf{x}_B,t)$ is the measured input current, $g(\mathbf{x}_C,\mathbf{x}_D;\mathbf{x}_A,\mathbf{x}_B,t)$ is the unknown impulse response of the earth, $r_{CD}(t)$ is the response of the recording system at the receiver, $n(k,\mathbf{x}_C,\mathbf{x}_D,t)$ is uncorrelated noise, k is the record number in the transmission sequence, $\mathbf{x}_A$ and $\mathbf{x}_B$ are the source electrode positions, $\mathbf{x}_C$ and $\mathbf{x}_D$ are the receiver electrode positions, and t is time.

The convolution of the input current with the response of the recording system is known as the system response:

$$s_{CD}(k,\mathbf{x}_A,\mathbf{x}_B,t) = i(k,\mathbf{x}_A,\mathbf{x}_B,t)^* r_{CD}(t). \quad (2)$$

Normally, the current is recorded using a device that is identical with that at the receiver, so the system response is known. The electric circuit consists of the transmitter, the cables to the electrodes, the electrodes themselves, and the earth. If there are inductive and capacitive effects in this circuit, the phase between the voltage across the transmitter terminals and the current in the circuit will be nonzero and will vary with frequency. That is, the input current may not follow exactly the prescribed function used to drive the transmitter. However, this has no bearing on the theory of the method because the current input to the earth and the response of the recording system are measured, and we use the measurement in the deconvolution, not the prescribed function.

The impulse response of the earth is obtained by deconvolving the measured voltage response for the measured system response. Deconvolution became an established data-processing tool in geophysics following Robinson (1957), who bases his work on the foundations laid by Wiener (1949) and Levinson (1947). Robinson (1967), Webster (1978), and Robinson and Osman (1996) show how methods have progressed in geophysics since. Our method is explained in Appendix A.

1D MODELING

Figure 2 illustrates a 1D earth model consisting of a 20 ohm-m half-space with a layer 25 m thick and resistivity of 500 ohm-m at a depth of 500 m. The source is a 1-A-m dipole, and the receiver is in line with the source electrodes at an offset of 1 km.

The black curve in Figure 3a shows the response of the 20 ohm-m half-space to a switch-on step, computed using the theory of Edwards (1997). There is an instantaneous rise at $t = 0$, followed by a

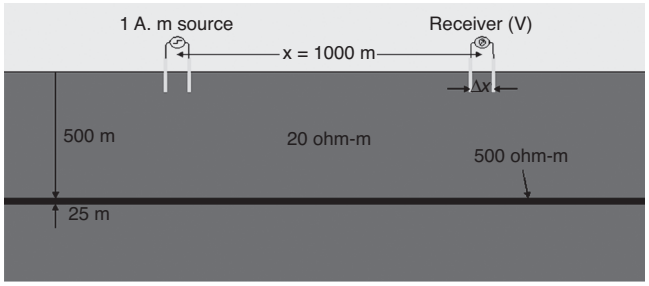

Figure 2. Model of a source and a receiver 1000 m apart at the surface of a 20 ohm-m half-space. At a depth of 500 m, a 25-m-thick layer is inserted with a resistivity that takes a value of 500 ohm-m if hydrocarbons are present and 20 ohm-m if they are absent.

slower rise to an asymptotic value equal to twice the value of the initial step. The initial step is a pure inductive effect; the current in the dipole creates a magnetic field that induces a voltage at the receiver position. The red curve in Figure 3a shows the effect of a 25-m-thick resistive layer of 500 ohm-m at a depth of 500 m; the amplitude of the response after the initial step is greater.

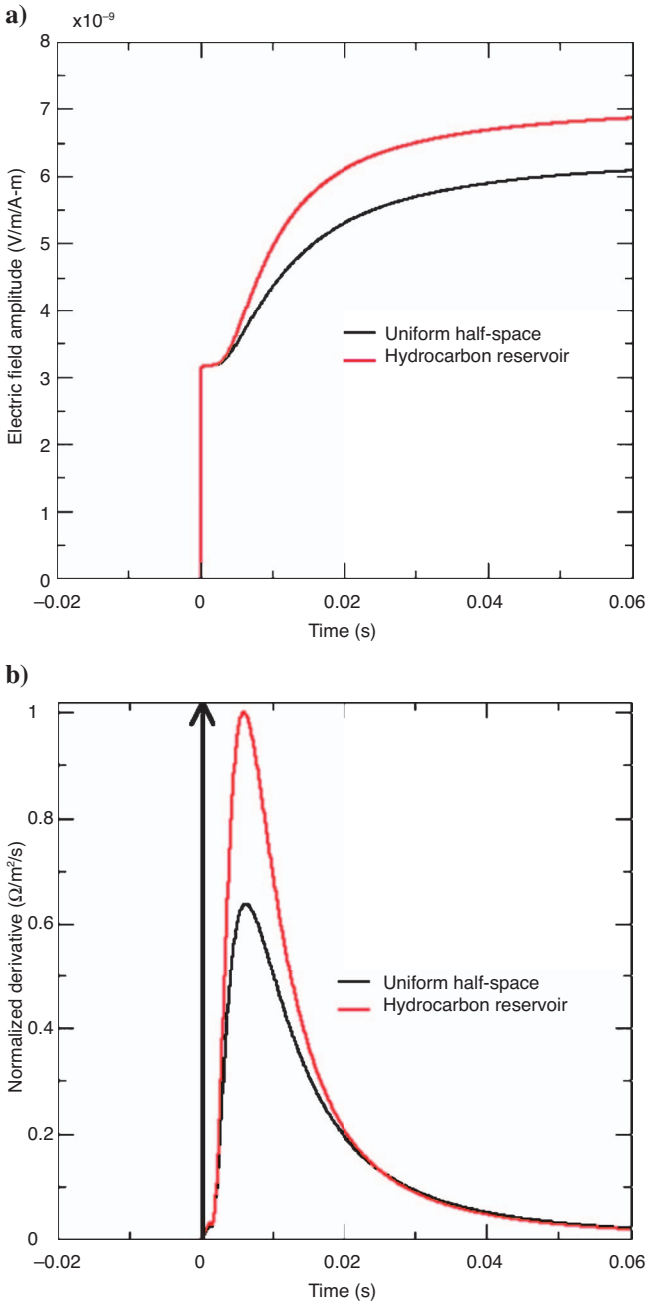

Figure 3. (a) Response of a 20 ohm-m half-space at an offset of 1000 m to a 1-A-m step at the source dipole (black curve) and with a 25-m-thick, 500-ohm-m resistive layer at a depth of 500 m (red curve). (b) Normalized impulse response, with normalization factor 3.433E + 6 for a 20 ohm-m half-space (black curve), with peak at 0.00628 s, and with a 25-m-thick, 500-ohm-m resistive layer at a depth of 500 m (red curve), with peak at 0.00585 s. The source and receiver are 1 km apart. The black vertical arrow at time = 0.0 represents the pure inductive effect of the impulse at the source.

Figure 3b shows the corresponding impulse responses obtained by differentiating Figure 3a. The initial step in Figure 3a, the airwave, becomes an impulse at $t = 0$ in Figure 3b, and the earth impulse response shows a rise to a peak at about 6.28 ms, followed by an asymptotic decay to zero. The influence of the thin resistive layer on the response is shown as the red curve, which has a significantly higher peak arriving at 5.85 ms — slightly earlier than the peak of the half-space response. Thus, the effect of the resistor can be seen in both the amplitude of the earth impulse response and the arrival time of the peak. These effects are seen at offsets greater than about twice the target depth.

Figure 3 is purely theoretical. In practice, the data are recorded with a band-limited recording system. The effect of this on the recorded response is simulated in Figure 4. The airwave becomes a sharp peak, and the peak of the earth response is smaller and follows the airwave; however, the peak of the earth response is larger when the resistor is present.

FIELD LAYOUT, EQUIPMENT, AND PARAMETERS

TOTAL chose the line of the MTEM profile and informed the University of Edinburgh and MTEM Ltd. that the crest of the reservoir was beneath the line at about 500 m depth. No other information about the extent of the reservoir or the subsurface structure was given. Several wellheads were in the area, which indicated the approximate horizontal location of the reservoir.

The layout of the north-south survey line is shown in Figure 5, with source and receiver electrode positions pegged at 100-m intervals. The object of the survey was to delineate, in a 2D sense, the subsurface resistor that corresponds to the stored gas.

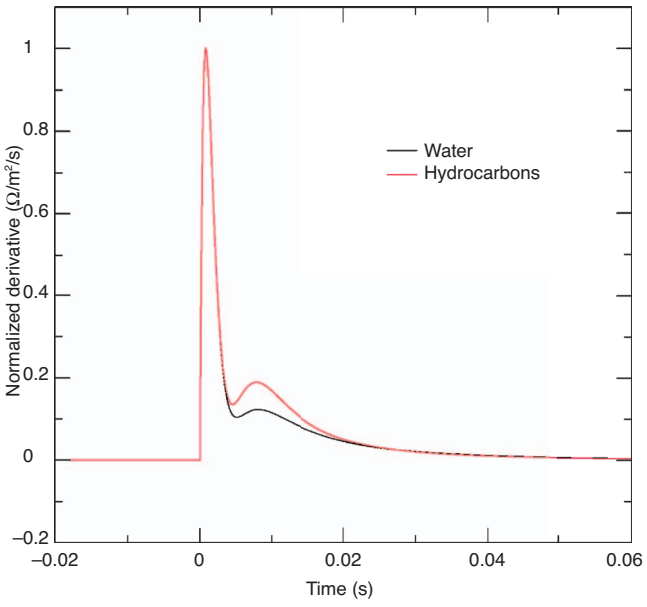

Figure 4. The result of convolving the responses in Figure 3 with a filter to simulate the recording system. The airwave becomes a sharp peak before the earth response. The impulse response has been normalized by its maximum value of $1.45158419 \times 10^{-6}$ V/m/A-m/s. The maximum values of the second peaks (normalized) are 0.12287 (water) and 0.18922 (hydrocarbons), giving a 54% increase in the response when hydrocarbons are present.

The field procedure consisted of switching a DC current between two source electrodes and recording the voltage responses at receiver locations along the line. The current source was a Zonge GGT-30 transmitter, powered by a ZMG-30 generator that switched DC current between opposite polarities. The time for the current to change polarity is on the order of microseconds, much shorter than the sampling interval used to record the data. The recording equipment was designed and built at the University of Edinburgh, in Scottish Enterprise Proof of Concept Project 4-ENO 004, to meet the specifications required by the MTEM method (Wright et al., 2002, 2005). Eleven two-channel recording units were made, ten for the receiving array and one to record the system response. Signal conditioning included a high-pass filter to attenuate very-low-frequency MT signals and a four-pole Butterworth antialias filter with a 6-dB point at two-thirds times the Nyquist frequency. A range of sampling rates was available, each with its own antialias filter.

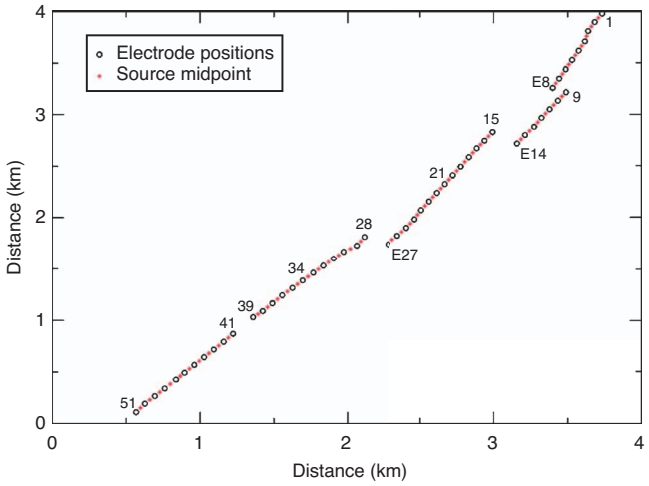

Figure 5. Layout of the line, showing source and receiver electrode positions pegged at 100-m intervals.

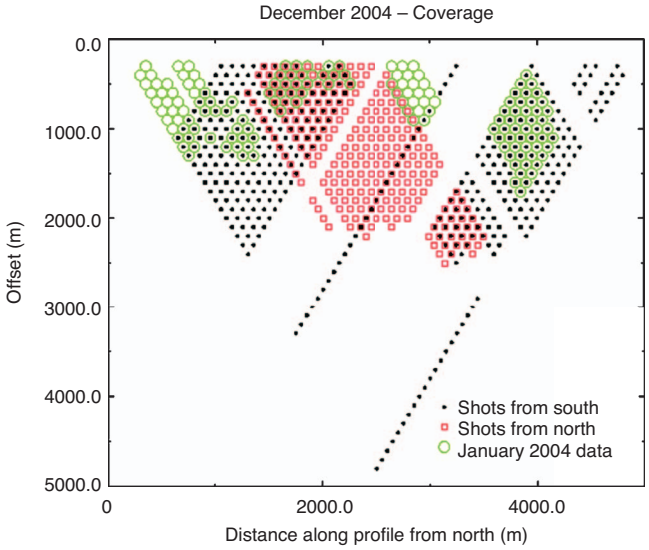

Figure 6. Data coverage in CMP-offset coordinates. Each point in the plot represents a single source/receiver pair, for which approximately 1500 transients were recorded.

Table 1. Data-acquisition parameters.

Parameter	
Frequency of current switch	1 Hz, 0.5 Hz
Amplitude of current switch	20–50 A
Voltage across source electrodes	750–1000 V
Record length	0.1 s
Sampling frequency	15 kHz
Number of records recorded per source position	1500–3000
Source electrode separation	100 m (normal), 300 m, 500 m
Receiver electrode separation, per channel	100 m

Each unit had its own global positioning system (GPS) receiver and onboard computers for analog-digital conversion, data recording and storage, and communication via fast transmission cable to a central recording workstation. Where communications were difficult across dense woods, independent GPS-synchronized recording workstations were used. A newly designed online quality control (QC) system enabled the layout and status of the system to be checked and the incoming data on all channels to be viewed simultaneously, before and after stack.

With the 10 receiver boxes and 100 m between a pair of receiver electrodes, a 2-km receiving spread was used, and the whole spread was shifted along the line with transient current input from the source from each end. The source was normally 100 m between current electrodes, and the offset between the source and nearest receiver was variable, as shown in Figure 6.

In principle, the source input current can be any time-varying signal. In practice, it is convenient to keep the load constant, so the current level is constant but switches polarity at predetermined times. For this survey, we used a simple step in current, reversing the polarity every second or half-second, for a 0.1-s record sampled at 15 kHz; that is, there were 1500 samples per record. The recording window was chosen such that steady state was reached before the end of recording at all offsets. The time between current reversals was much longer than the record length, so we recorded the step response each time. For later surveys, we used pseudo-random binary sequences (PRBS) rather than steps because this approach improves efficiency. Our real-time QC system allowed us to see how the step responses stacked up. We found that we needed to record about 1500 responses at each source position to achieve adequate signal-to-noise ratio (S/N) at all offsets. The parameters are summarized in Table 1.

Figure 6 shows the data coverage in common-midpoint (CMP) offset coordinates. The horizontal vector positions of the source and receiver electrodes for a given source/receiver pair are $\mathbf{x}_{S1}$, $\mathbf{x}_{S2}$, $\mathbf{x}_{R1}$, and $\mathbf{x}_{R2}$; the corresponding midpoint and offset are defined as

$$\mathbf{x}_{CMP} = (\mathbf{x}_{S1} + \mathbf{x}_{S2} + \mathbf{x}_{R1} + \mathbf{x}_{R2})/4, \quad (3)$$

$$x_{offset} = \left| \frac{(\mathbf{x}_{S1} + \mathbf{x}_{S2})}{2} - \frac{(\mathbf{x}_{R1} + \mathbf{x}_{R2})}{2} \right|. \quad (4)$$

As in seismic reflection, each CMP is shared by several source/receiver pairs. Note that the offset is the modulus of the source/receiver separation; that is, we assume the reciprocity principle. In

fact, we use this principle to check the quality of our data acquisition and processing.

DATA PROCESSING AND RECIPROCITY

For each switch of the transmitter, a 1500-sample, 0.1-s transient response of each channel was recorded. Data processing analyzed the 8 GB of recorded data for noise bursts and identified unacceptable transients (approximately 10%). The accepted data were treated for 50-Hz noise removal, deconvolved for the recorded system response, and stacked to recover the impulse response. The result was then filtered with a zero-phase Gaussian filter of the form $\exp\{-\alpha^2 f^2\}$, in which f is frequency, with e^{-1} cut-off frequency α^{-1} varied with source/receiver offset to recover a band-limited estimate of the impulse response $g(\mathbf{x}_s,\mathbf{x}_r,t)$.

The deconvolution compensates for the variation in current at the source for each transient response and for each source position. The received voltage is also proportional to the separation between source electrodes and the separation between receiver electrodes. The data are scaled at the deconvolution stage to compensate for these effects, such that the integrated impulse response is what would be obtained for a 1 A-m step. The zero-phase filtering is designed to have no effect on the late-time values of the integrated impulse responses.

The reciprocity principle can be expressed mathematically as

$$g(\mathbf{x}_A,\mathbf{x}_B;\mathbf{x}_C,\mathbf{x}_D,t) = g(\mathbf{x}_C,\mathbf{x}_D;\mathbf{x}_A,\mathbf{x}_B,t). \qquad (5)$$

That is, the impulse response of the earth is invariant when the positions of source and receiver are interchanged. Our data set contains numerous examples of this reciprocity principle, and we used it to check our data quality. Figure 7 shows one typical example: The two impulse responses lie on top of each other, apart from small uncorrelated differences that we attribute to noise. This result is obtained because the S/N is good and the deconvolution is performed correctly.

This check is not foolproof. If, for example, the source measurement were always divided by a factor of two in the processing flow, the reciprocal impulse responses would still be identical, but both would be too big by a factor of two. To guard against mistakes of this kind, we have instituted a check on the processing flow using identical signals at the source and receiver: The impulse response should be a band-limited impulse with integral equal to unity.

ERRORS AND NOISE

The measurements we make are subject to errors. We account for these errors by the noise term in equation 1. In an analysis of the fit of modelled results to our measured data, it is normal practice to define the uncertainty of the measurements using a statistical model of the errors (e.g., Parker, 1994). Such models make assumptions about the probability distribution of the errors. One such commonly used assumption is that the errors are a random-noise process and the probability distribution function (PDF) of the errors is the normal or Gaussian distribution.

Random errors, however, are extremely small compared with the main sources of noise in our data, which are very often cultural noise such as power-line and railway noise. Such noise is not random: It often consists of a fundamental frequency, say, 50 Hz in Europe or 60 Hz in North America, plus harmonics — typically odd harmonics — and often there are fluctuations in the value of the fundamental frequency. Appendix B describes our approach to suppressing cultural noise. Appendix C describes a conventional error analysis of the data after processing to suppress cultural noise.

RESULTS

Real-time analysis

We have developed two useful tools to obtain a quick look at subsurface resistivity: (1) common-offset displays of the recovered impulse responses (or any transformation of them) and (2) an apparent resistivity section based on the arrival times of the peaks of the impulse responses. These two types of display can be made within about a day of finishing a line.

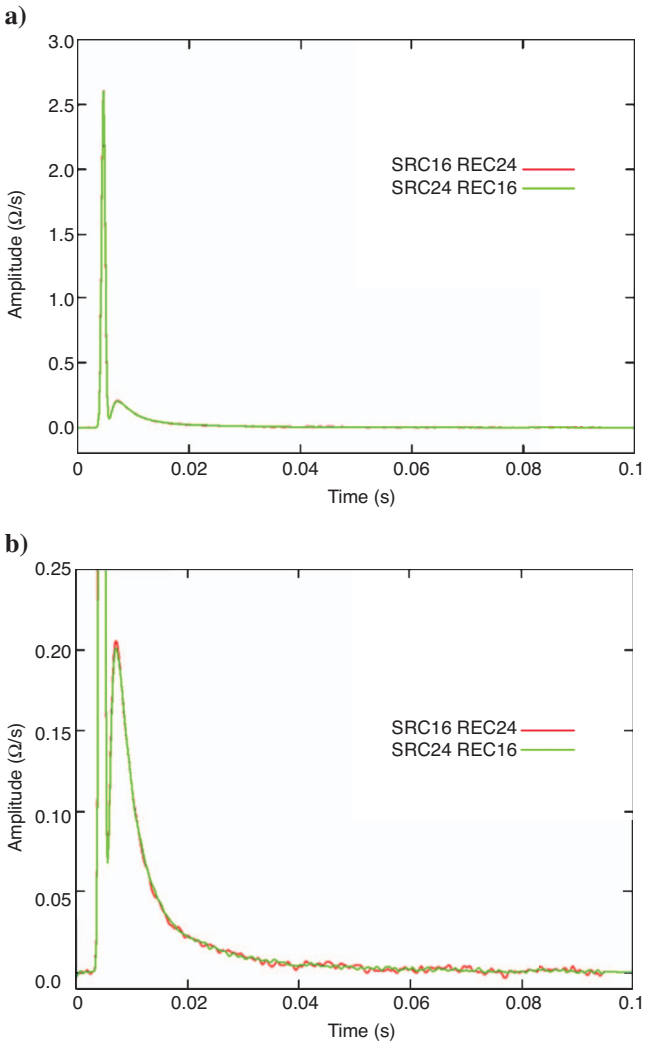

Figure 7. Estimates of the earth impulse response (a) and (b) are the same data with different vertical scales. There has been no division by source and receiver bipole lengths. In red, the source electrodes were at pegs 16 and 17 with the receiver electrodes at pegs 24 and 25; in green, the source electrodes were at pegs 24 and 25, and the receiver electrodes were at pegs16 and 17. The sharp peak at 5 ms is the airwave, corresponding to the current switch 5 ms after start of data. The earth impulse response follows and is almost identical for the two estimates, the rms difference being 0.00025 ohm/s.

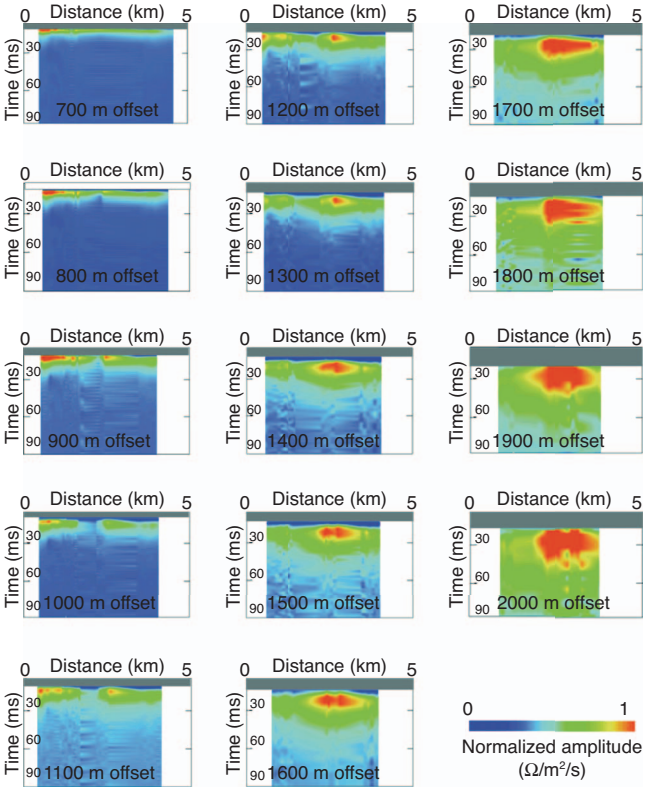

Figure 8. Common-offset sections of the earth impulse response function for offsets 700–2000 m. The horizontal coordinate is the midpoint between source and receiver, and the scale is shown at the top of each figure; the vertical coordinate is time, with the complete axis being 0–100 ms. The gray bar at the top of each section shows where the airwave has been muted out. The relative amplitude scale is denoted by the color bar. The airwave has been muted out. The presence of a deep (>500 m) resistor can be seen at offsets of about 1400 m and greater.

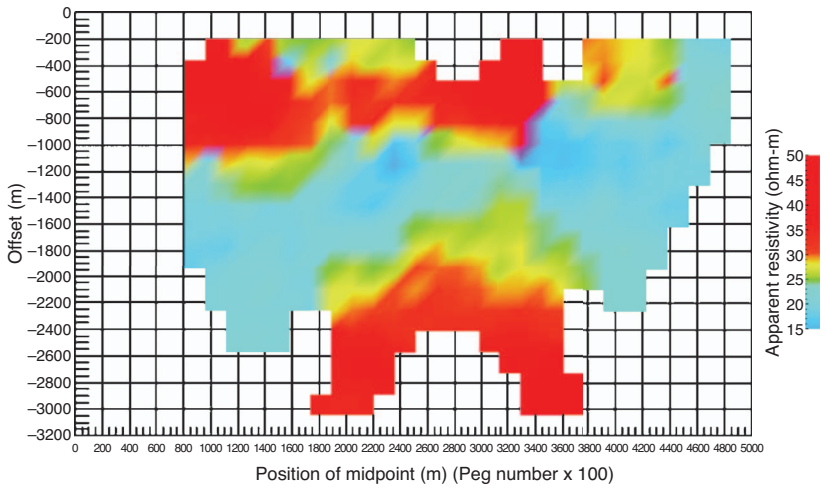

Figure 9. Traveltime-to-resistivity mapping in CMP-offset coordinates using equation 7; horizontal distances are measured from peg 1 in the north.

Figure 8 shows the impulse response data displayed as a series of common-offset sections. Each section displays the impulse response data of a single horizontal line in Figure 6. We know that the presence of a resistor is manifested by increased amplitude and earlier arrival of the peak of the earth impulse response. Figure 8 displays the amplitudes. The effect of a resistor is noticeable at offsets greater than about twice its depth. In Figure 8 we see high amplitudes between pegs 18 and 40 (horizontal distances of 1800–4000 m from the north) at offsets of about 1400 m and greater. We interpret this as the effect of the resistor corresponding to the known gas at a depth of 500 m and greater.

We can use the traveltime of the peak as well as the amplitudes. Appendix D shows that the arrival time of the peak for a uniform half-space is given by

$$t_{\text{peak},r} = \frac{\mu r^2}{10\rho}, \tag{6}$$

where $\mu = 4\pi 10^{-7}$ H/m, r is offset in meters, and ρ is resistivity in ohm-meters. For example, with $r = 1000$ m and $\rho = 20$ ohm-m, $t_{\text{peak},r} = 2\pi 10^{-3}$, as shown in Figure 3b. Equation 6 can be rearranged to define an apparent resistivity:

$$\rho_H = \frac{\mu r^2}{10 t_{\text{peak},r}}, \tag{7}$$

in which ρ_H is the apparent resistivity of the half-space that yields the same peak arrival time at offset r as the data.

This new apparent resistivity is a useful addition to the list of apparent resistivities given by Spies and Eggers (1986). Using this simple formula on each recovered impulse response, we make the display shown in Figure 9, in which there is a deep resistor between pegs 18 and 40 (horizontal positions 1800–4000 m) overlain by a conductor and variable near-surface resistors. This interpretation is consistent with the results of the common-offset sections.

The theory used to derive equation 7 is based on a dipole source, that is, a point source. We are using bipole sources with a finite separation between the poles. In practice, a bipole behaves like a dipole at distances greater than about five times the bipole length. In this survey, we worked within this rule of thumb.

It would be interesting to map from offset to depth, but this is not straightforward. The problem can be understood by considering Figure 10. The colored curves are obtained using equation 6 for different resistivities. The black circles are traveltime peaks as a function of offset for CMP 3600. For offsets 900–1100 m, the increase in traveltime with offset, or moveout, is large, indicating low resistivity. At 1100 m, the data point circled in red, there is an abrupt change in slope and the moveout is less steep, indicating more resistive material. The equivalent half-space resistivity for the circled data point lies between the 10 and 20 ohm-m curves, so it is about 15 ohm-m.

This is the value returned by equation 7 and plotted in Figure 9. However, from the average slope between 1100 and 1700 m, it is clear that the resistivity is much greater — perhaps 60 to 80 ohm-m.

Clearly, we should be using the slope to estimate the equivalent half-space resistivity. That is, we differentiate equation 6 to yield

$$\frac{dt_{\text{peak},r}}{dr} = \frac{\mu r}{5\rho} \tag{8}$$

and rearrange this formula to give another new apparent resistivity,

$$\rho_I = \frac{\mu r}{5}\left(\frac{dt_{\text{peak},r}}{dr}\right)^{-1}. \tag{9}$$

The relationship between ρ_H and ρ_I is roughly analogous to the relationship between stacking velocity and interval velocity in the analysis of seismic reflection data. So we refer to ρ_I as the apparent interval resistivity.

We have tried to extract apparent interval resistivities because these would have higher vertical resolution than the apparent half-space resistivities, but we have not been able to make this work on these data. The reason is that errors in the estimates of the peak traveltimes are increased by noise. To compute the slope requires at least two traveltimes, each with errors, and our data are not good enough to make this computation. With improved data acquisition, we expect to make this work on data in the future.

Integration of impulse responses to recover step responses

The impulse responses may be integrated to give step responses. Figure 11 shows a real data example of a step response. At late times, the curve rises slowly and is asymptotic to some value V_∞. An estimate of V_∞ may be made by fitting an appropriate curve to the data at late times. V_∞ is in fact the DC value that would be obtained for a 1 -A-m source; thus, the apparent resistance is V_∞ ohm.

We may estimate one value of the apparent resistance for each source-receiver pair and, knowing the positions of the source and receiver electrodes, use a standard DC resistivity inversion routine, such as described by Loke and Barker (1996), to obtain an estimate of subsurface resistivities. The result of this inversion for these data is shown in Figure 12. This is quite a nice result, especially as it clearly shows the top of the reservoir and is consistent with the results of real-time analysis. One shortcoming is that it does not show the bottom of the reservoir.

In the standard terminology of DC resistivity, a dipole-dipole array has the same spacing a between current electrodes and between potential electrodes, and the distance between the closest current and potential electrodes is denoted by na. The spread length is thus $(n + 2)a$. Conventionally, n-factors up to about six are used, the S/N for larger values being generally too small for a meaningful measurement (Dahlin and Zhou, 2004). However, DC values derived from MTEM measurements can use much larger values of n because of the increase in S/N obtained by the data processing. In this study, values up to $n = 25$ were used. According to Edwards (1977), the penetration depth for the dipole-dipole array with large n values lies between 0.239 and 0.250 times the length of the array, making it 645–675 m. This is in agreement with Figure 12. To see beneath the reservoir with this method, we would need to use a longer spread length.

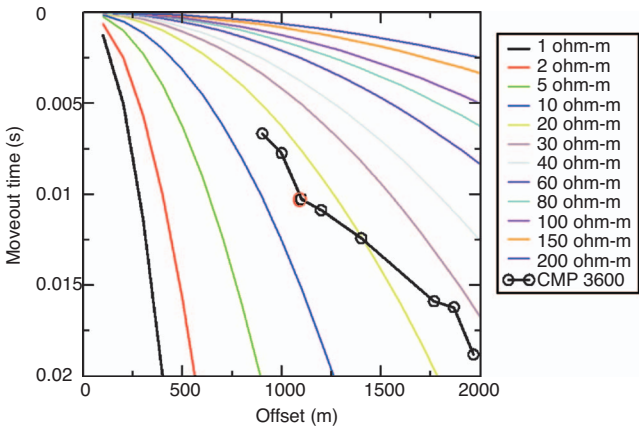

Figure 10. Times of earth impulse response peaks plotted against offset. The black circles are data points from CMP position 3600. The colored lines are plots of peak time versus offset, using equation 6 for different values of resistivity. The traveltime data show a clear break in the slope at an offset of 1100 m — at the data point circled in red — indicating the presence of a resistor.

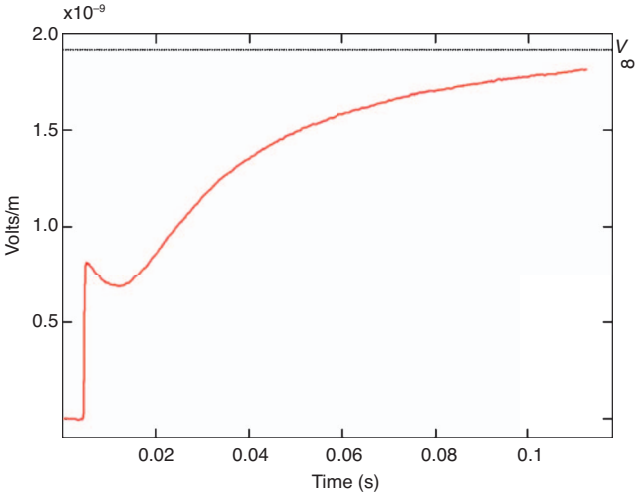

Figure 11. Real-data example of an integrated impulse response, or step response. At late times, the curve rises slowly and is asymptotic to some value V_∞.

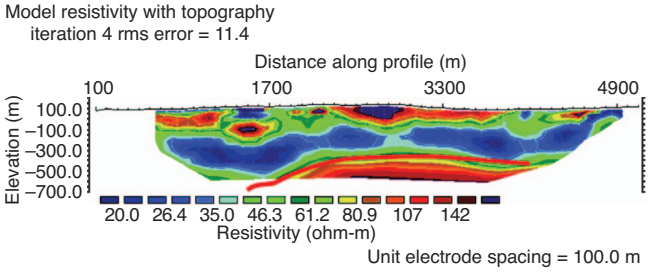

Figure 12. Two-dimensional dipole-dipole DC resistivity inversion of the MTEM data using the estimated asymptotic values of the step responses. The red curve shows the top of the reservoir.

Collated 1D inversions of CMP gathers

The traditional approach to interpreting EM data is to use inversion. We have developed a simple approach using 1D inversion. We arrange our step response data in CMP gathers and try to find a single stratified (one-dimensional) earth model whose step responses at the same offsets fit the data. Each CMP gather is treated independently. The inversion results from each CMP are displayed side by side to form a 2D section.

The layered model has fixed boundaries, and the parameters are the layer resistivities. We may choose a parameterization in which the layer thicknesses are constant or increase logarithmically. As offset increases within a CMP gather, the corresponding step responses are sensitive to layers at increasing depth. We adopt, in general, a linear scale for depth and a logarithmic scale for resistivity for direct comparison with both well-log information (if there is any) and interpreted seismic cross sections (if there are any). However, the variation in resistivity values found in this survey is much less than one order of magnitude, so the model results are best displayed with a linear depth scale and a linear resistivity scale. A typical model has 20 layers of equal thickness overlying a uniform half-space.

We find this parameterization enables the inversion scheme to recover a resistive layer in synthetic models and resolves resistive target layers, as in this paper. No a priori information is used (in fact, we had none); the starting model is a uniform half-space. A full waveform multioffset Occam inversion has been developed, based on the work of Constable et al. (1987), and this finds the smoothest model that satisfies a collection of offset data within a CMP gather. Convergence occurs in about four to eight iterations.

A key issue in the inversion is what is known as static shift. There are lateral resistivity variations, especially in the near surface, that clearly are not included in a 1D model. Compensation for these variations can be made in a number of ways. One is to adopt the method of Newman (1989) for transient EM with a grounded source and a magnetic receiver, whereby a multiplicative scaling factor is determined that leads to a minimum rms inversion model. An alternative is to impose an approximation that the amplitude within a CMP gather falls off such as $(1/\text{offset})^3$, the theoretical value for a half-space (Weir, 1980), and to scale accordingly. The second method is adopted here.

Illustrative full-waveform, multioffset inversion results are shown in Figures 13 and 14. Figure 13a shows models derived at several CMP locations to the northeast of the profile (pegs 11–15), and Figure 13b displays models over the central section of the profile

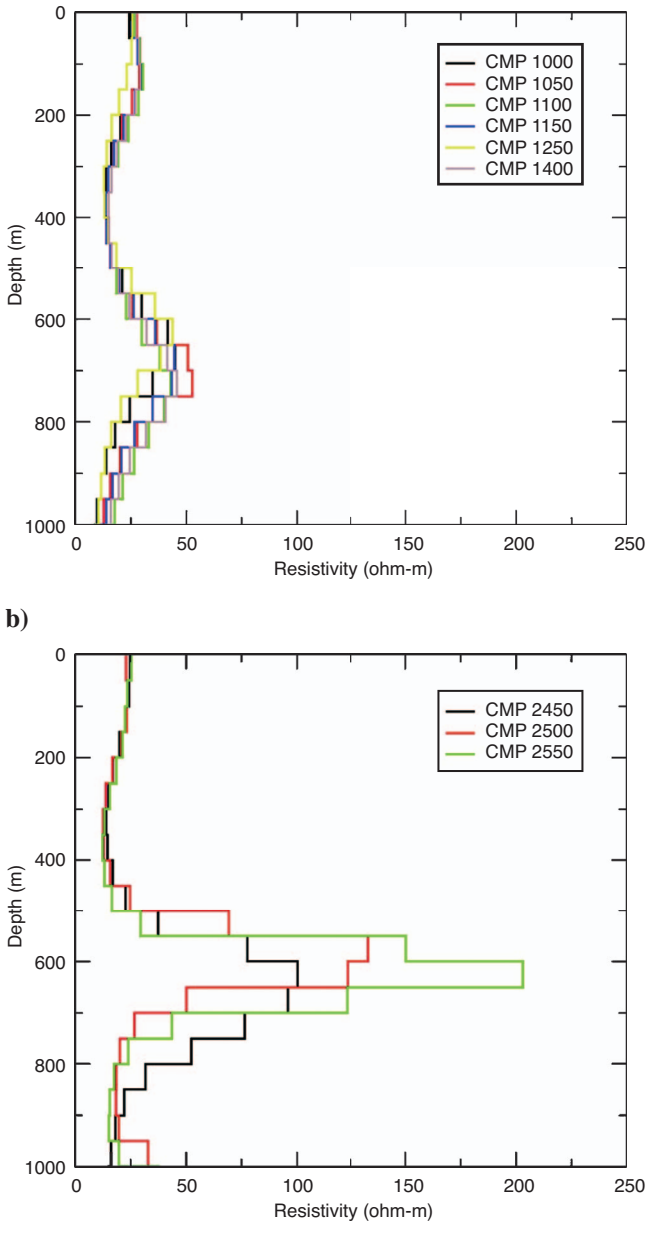

Figure 13. (a) Resistivity models obtained by full-waveform multioffset inversion at CMP positions 1000–1400. (b) Resistivity models obtained by full waveform multioffset inversion at CMP positions 2450–2550.

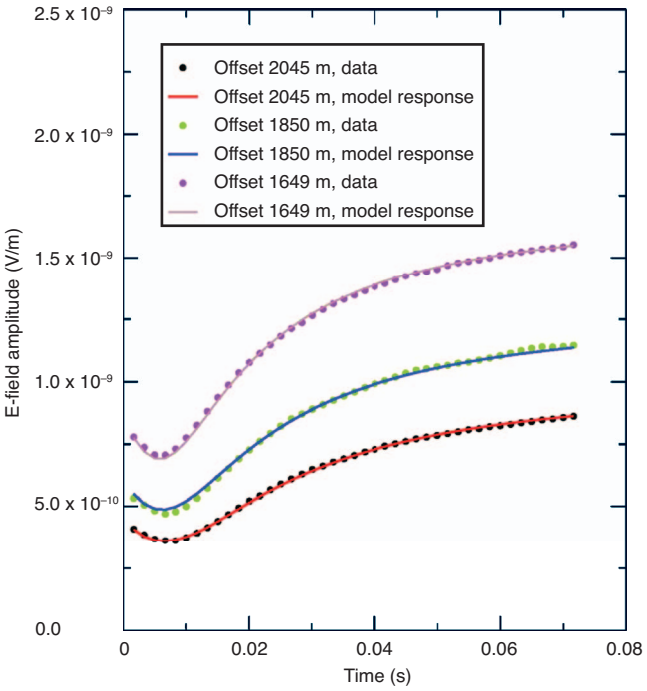

Figure 14. Step-response data and modelled responses at CMP position 2500.

(around peg 25). The derived structures are similar to a depth of around 500 m, but thereafter the models depart significantly. Over the central and southwest sections, a resistive layer is seen in all models, with resistivity values between 100 and 200 ohm-m. To the northeast, the resistivity of the corresponding layer is less than 60 ohm-m. Between 500 and 700 m depth, the transverse resistance in the central section is around 20,000 ohm-m^2, in contrast to around 6400 ohm-m^2 to the northeast.

To execute an inversion routine, uncertainties must be included for each data point. Appendix C shows that, on average, errors in the step response are a fraction of 1% of their value. Inversion using 1D modeling is unable to represent data obtained in the 3D world to that level of accuracy. Instead, one-standard-deviation error bars are set to 1% of the amplitude of the step function at each time sample. The corresponding standard chi-squared misfit, whose expected value is unity, is shown in Table 2 for the CMP positions displayed in Figure 13a and b. The expected value of chi-squared is one, so these misfits indicate that an error allocation of 1% of the step function amplitude is reasonable. An example of the fit to multitrace data is shown in Figure 14 for three offsets at CMP position 2500, with a misfit of 3.12 as in Table 2.

The result of collating all of the 1D inversions is shown in Figure 15. The resistor corresponding to the known gas is in red, and its top and bottom are clearly delineated. There is some ambiguity in the inversion because the earth's response depends partly on the transverse resistance of a layer, that is, the product of its thickness and resistivity. For example, a 10-m-thick layer of 200 ohm-m resistivity has the same transverse resistance as a 20-m-thick layer with 100 ohm-m resistivity. However, the response also depends strongly on the position of such a resistive layer. Thus, the results of Figure 15 give a good indication of the top and bottom of the layer, with vertical uncertainties on the order of the layer thickness used — in this case, 50 m.

Table 2. Chi-squared misfit of inverted models to data for various CMP positions.

CMP Position	Chi-squared misfit
1000	1.49
1050	1.42
1100	1.10
1150	1.31
1250	2.18
1400	0.60
2450	0.93
2500	3.12
2550	2.58

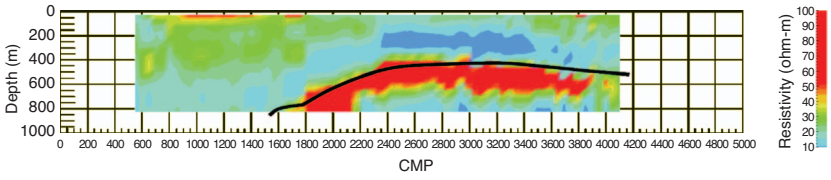

Figure 15. Collated 1D full-waveform inversions of CMP gathers of the step-response data. The black curve shows the top of the reservoir.

CONCLUSIONS

The data we collected with very limited equipment are of good quality and are sufficient, with simple processing, to show the apex of the gas reservoir. Each of the 522 data points shown in Figure 6 represents an impulse response of 1500 samples. Recovery of the impulse responses requires a significant effort to suppress cultural noise, which is generally of much greater amplitude than any random noise component. Appendix B provides the details. Appendix C shows that the step responses are determined with an uncertainty of a fraction of 1% of their value.

To interpret the data, we have developed four different approaches that are consistent with each other, which is very encouraging. Two of these methods — display of common-offset sections and mapping of peak arrival time to equivalent half-space resistivity — may be performed quite quickly after the data have been recorded. The second method uses a new apparent equivalent half-space resistivity, defined by equation 7. A formula for apparent interval resistivity (equation 9) has also been derived, but we did not succeed in applying it to these data.

The integration of the impulse responses to generate step responses allowed us to estimate the DC value and use standard 2D dipole-dipole DC resistivity inversion of the data, which found the top of the resistor corresponding to known gas. Both the top and bottom of the reservoir were identified using a series of full-waveform multioffset 1D Occam inversions performed independently on the step responses of individual CMP gathers. No constraints were used in the inversion, and the vertical uncertainty in the position of the resistive layer was about 50 m.

The results demonstrate that the MTEM method has the potential to be used as an exploration tool for hydrocarbons. A particular application of the method is where a potential hydrocarbon reservoir has been identified using other geophysical methods, e.g., seismic reflection, and there is a need to reduce the risk of drilling a dry well.

ACKNOWLEDGMENTS

We thank TOTAL for inviting the University of Edinburgh and MTEM Ltd. to test the MTEM method at the gas storage site. We also thank TOTAL for very generously arranging the permitting with landowners at the site, switching off the cathodic protection while we were surveying, and providing the position of the top of the reservoir shown in Figures 12 and 15. The recording system and the data-processing flow were developed under Proof of Concept Project 4-ENO 004, funded by Scottish Enterprise. We thank the University of Cologne for the loan of their generator and Zonge switch box. We thank Pierre Andrieux, two anonymous reviewers, and Kerry Key, associate editor, for their very helpful comments on our paper. This paper is published with the permission of the executive directors of MTEM.

APPENDIX A

DECONVOLUTION

Combine equations 1 and 2 and simplify:

$$v(t) = s(t) * g(t) + n(t), \tag{A-1}$$

in which $v(t)$ and $s(t)$ are known. In general, $s(t)$ is not close to an impulse $\delta(t)$, so the convolution $s(t)^* g(t)$ is not close to the impulse response. The objective of deconvolution is to replace $s(t)$ with an impulse.

Transform equation 1 from the time domain to the frequency domain:

$$V(\omega) = S(\omega)G(\omega) + N(\omega), \tag{A-2}$$

in which, as the result of the convolution theorem, the convolution becomes a multiplication. At this point, the obvious step is to divide by $S(\omega)$, but this is numerically unstable because the noise blows up at frequencies where $|S(\omega)|$ is small. Instead, we multiply by

$$F(\omega) = \frac{S^*(\omega)}{|S(\omega)|^2 + \varepsilon} \approx \frac{1}{S(\omega)}, \tag{A-3}$$

in which the asterisk denotes complex conjugate and ε is a small positive constant. The denominator is real, and ε prevents division by zero where $|S(\omega)|$ is small. This is still not perfectly satisfactory as it does not recognize the inherent bandwidth limitation of the system. As a finishing touch, we apply a zero-phase filter of the form

$$D(\omega) = \exp\left(-\left(\frac{\omega}{\omega_0}\right)^2\right). \tag{A-4}$$

The Fourier transform of $D(\omega)$ is $d(t)$:

$$d(t) = \sqrt{\pi}\omega_0 \exp\{-\pi^2\omega_0^2 t^2\}. \tag{A-5}$$

This is a band-limited approximation to a delta function, $\delta(t)$; it has a peak at $t = 0$ and its integral is unity:

$$\int_{-\infty}^{\infty} d(t)dt = 1. \tag{A-6}$$

Multiplying equation A-2 by $F(\omega)$ and $D(\omega)$ gives

$$\begin{aligned} F(\omega)D(\omega)V(\omega) &= F(\omega)D(\omega)S(\omega)G(\omega) + F(\omega)D(\omega)N(\omega) \\ &\approx D(\omega)G(\omega) + F(\omega)D(\omega)N(\omega). \end{aligned} \tag{A-7}$$

Finally, transforming back to the time domain gives

$$\begin{aligned} f(t) * d(t) * v(t) &= f(t) * d(t) * s(t) * g(t) \\ &\quad + f(t) * d(t) * n(t) \approx d(t) * g(t) \\ &\quad + f(t) * d(t) * n(t) \\ &\approx \delta(t) * g(t) + f(t) * \delta(t) * n(t) \\ &= g(t) + f(t) * n(t). \end{aligned} \tag{A-8}$$

Comparing equations A-1 and A-8, we see that the objective of replacing $s(t)$ by an impulse has almost been achieved; but because of the presence of noise, we have had to settle for a band-limited impulse. The noise is still present but has been controlled. The angular frequency ω_0 at which $D(\omega)$ decays to $1/e$ is normally chosen to be half the angular Nyquist frequency:

$$\omega_0 = \frac{\pi}{2\Delta t}. \tag{A-9}$$

APPENDIX B

SUPPRESSING CULTURAL NOISE

We use two methods to reduce the effects of cultural noise: signal polarity reversals and filtering.

Signal polarity reversals

Let the voltage measurement for the kth transient in the sequence be

$$v(k,t) = m(k,t) + cn(k,t) + rn(k,t), \tag{B-1}$$

where $m(k,t)$ is the signal we want to measure, $cn(k,t)$ is cultural noise (typically 50 Hz plus harmonics or 60 Hz plus harmonics), and $rn(k,t)$ is random noise. Normally, the random noise is very small compared with the cultural noise. We now make a repeat measurement at time T later, only this time the input current is reversed so the response is reversed. We have

$$\begin{aligned} v(k+1,t-T) &= m(k+1,t-T) + cn(k+1,t-T) \\ &\quad + rn(k+1,t-T). \end{aligned} \tag{B-2}$$

We assume the earth has not changed, so the earth response in equation B-2 is the same as that in equation B-1 except that its polarity is reversed, that is,

$$m(k+1,t-T) = -m(k,t). \tag{B-3}$$

We expect the cultural noise to be periodic and choose T to be a multiple of the period; for example, $T = 1$ s is one possibility for 50- and 60-Hz noise. Then, ideally,

$$cn(k+1,t-T) = cn(k,t). \tag{B-4}$$

Subtracting equation B-2 from equation B-1 and dividing by two gives

$$\begin{aligned} &\frac{v(k,t) - v(k+1,t-T)}{2} \\ &\quad = m(k,t) + \frac{rn(k,t) - rn(k-1,t-T)}{2}. \end{aligned} \tag{B-5}$$

Thus, the cultural noise is eliminated, and the signal and the incoherent random noise in both measurements remain. This procedure obviously relies on the cultural noise being periodic. The procedure may be repeated as often as necessary. Odd traces have one polarity; even traces have reversed polarity.

Figure B-1 illustrates the procedure. The first measurement, corresponding to equation B-1, is green; the second measurement, with reversed polarity, is red; and the stack of the two, corresponding to equation B-5, is black. It is clearly a step response plus noise. If the signal polarity is not reversed, stacking two even traces or two odd traces (summing them and dividing the result by two) does not pro-

duce any discernible increase in S/N. The step response is invisible, as it is on either of the prestack traces of Figure B-1.

These examples show that polarity reversal is an important weapon in suppressing cultural noise.

Filtering

The cultural noise component usually has a known fundamental frequency and harmonics, each of which has an amplitude and a phase and can be plotted as a vector in the complex plane. The phase of any component of the noise is unlikely to be the same as the phase of the signal at the same frequency, and the sum of the two components at that frequency will have a phase not equal to the phase of either component.

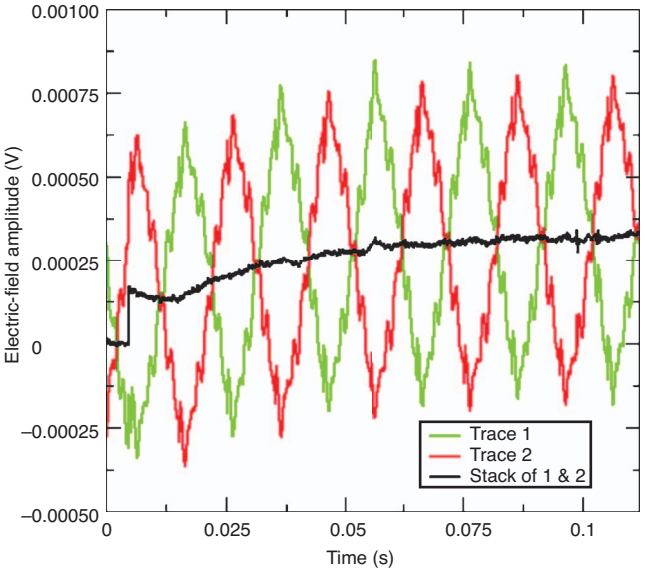

Figure B-1. Two consecutive raw traces after reversing the polarity of one to correct for the source polarity are shown in green and red. The result of stacking these two traces is shown in black.

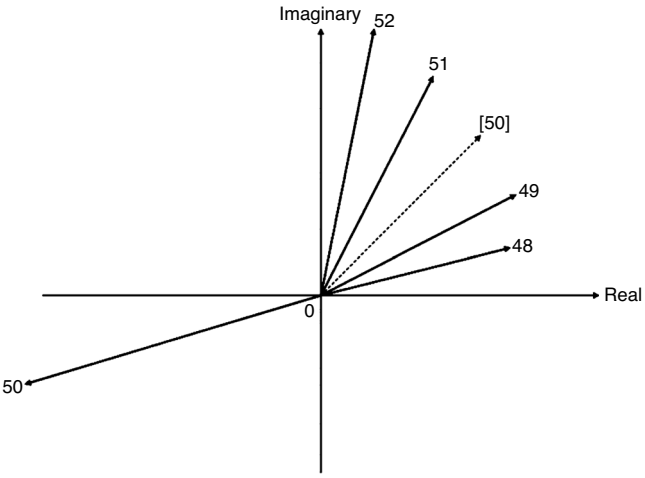

Figure B-2. Diagram to show the effect of 50-Hz cultural noise on the spectral components from 48–52 Hz. The solid vectors represent the data before filtering; after filtering, only the 50-Hz component has changed, shown by the dashed vector.

Figure B-2 shows a possible situation in which the transient response is 1 s long, so its frequency components are at 1, 2, 3, etc., Hz. The vectors of the 48-, 49-, 50-, 51-, and 52-Hz components might look as shown by the solid vectors in Figure B-2, with the 50-Hz vector not conforming to the pattern of the others. If the data have been sampled properly, the amplitude and phase of the earth response are both smoothly varying functions. The 50-Hz vector is too big and has the wrong phase. We attribute this behavior to the noise contribution, known to be at 50 Hz, and conjecture that the signal vector should be somewhere between the vectors for 49 and 51 Hz, which we expect to be composed of signal plus random noise. We find the magnitude and phase of the 50-Hz signal vector by interpolation, as shown schematically by the dotted vector.

APPENDIX C

ERRORS

To obtain an estimate of the error present in the processed data, we consider the data as consisting of stacks of pairs of consecutive raw traces, as described in Appendix B. This is because we alternate the polarity of the source signal. The standard error on the mean $\sigma_m(t)$ for traces from a single-source receiver was calculated using the equation

$$\sigma_m(t) = \frac{\sigma(t)}{\sqrt{N}}, \tag{C-1}$$

where $\sigma(t)$ is the standard deviation of the population and N is the number of pairs of traces in the population. Figure C-1 shows the stacked step response with plus and minus one standard error of the mean. The error on the stacked step response is extremely small. Figure C-2 shows the standard error on the mean for this trace as a percentage of the amplitude of the step response. On average, the error of the stacked response is less than 0.4%.

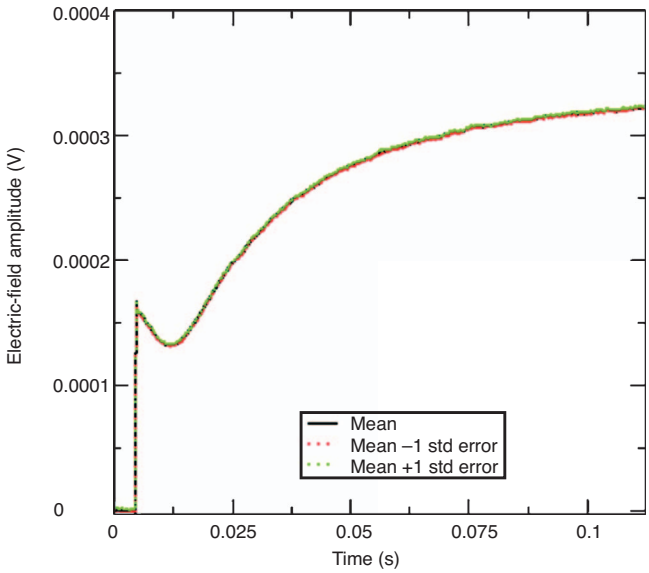

Figure C-1. The black line shows the step response recovered from processing 1800 raw traces. The green and red lines, respectively, denote plus and minus one standard error on the mean.

A measure of data quality can be made by calculating the S/N as follows. The noise is taken as the rms amplitude of the pretrigger samples before the source switches, and the signal is taken as the late-time amplitude of the step. The data shown in Figure C-1 have a S/N of 57 dB, that is, the pretrigger noise is 0.14% of the late-time mean value, consistent with Figure C-2. In general, data are considered to be good if the S/N is greater than about 45 dB. Figure C-3 shows the S/N for all the data collected in the survey.

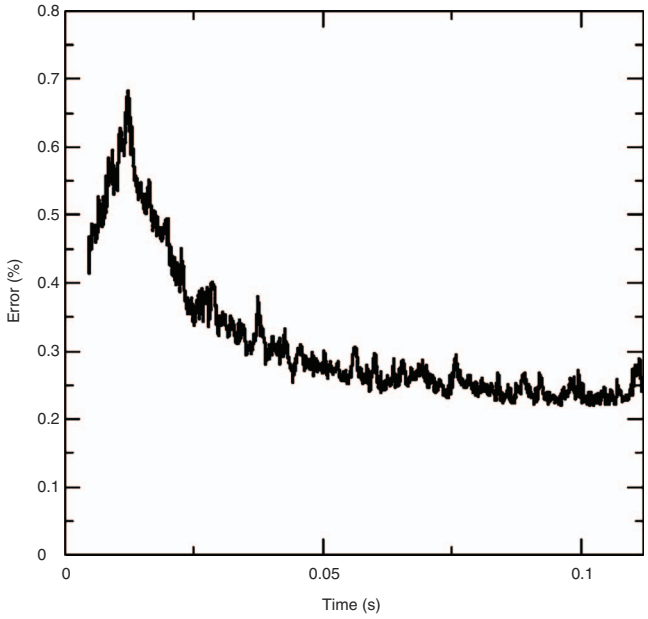

Figure C-2. The standard error on the mean as a percentage of the amplitude of the stacked step response.

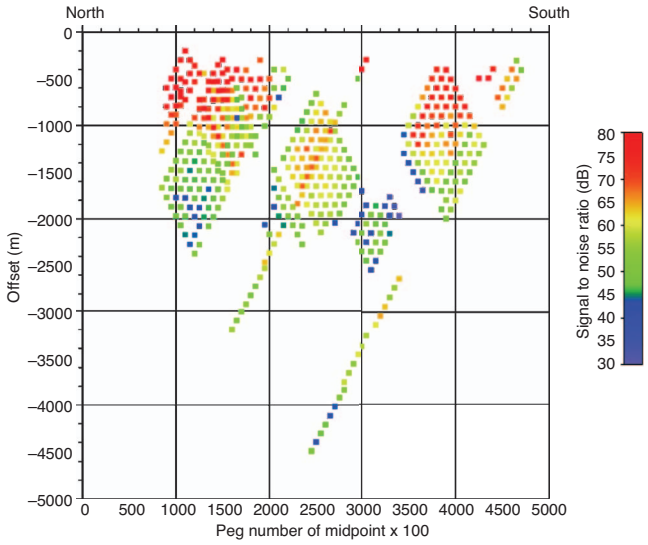

Figure C-3. A plot similar to Figure 6 but showing the S/N of all data.

APPENDIX D

DETERMINATION OF TIME TO THE PEAK OF THE EARTH IMPULSE RESPONSE

The inline electric-field response at the surface of a half-space of resistivity ρ ohm-m to a switch-off 1-A-m step in current at a dipole at a distance r is given by Weir (1980):

$$E(\sigma,r,t) = \frac{1}{2\pi r^3}\left[erf\left(\frac{r}{c2\sqrt{t}}\right) - \frac{2}{\sqrt{\pi}}\frac{r}{c2\sqrt{t}}\exp\left(-\frac{r^2}{c^2 4t}\right)\right], \tag{D-1}$$

in which $c^2 = \rho/\mu$, $\mu = 4\pi 10^{-7}$H/m, and erf is the error function. The response to a unit impulse is obtained by differentiating equation D-1 and multiplying by −1, as derived by Wilson (1997):

$$g(\rho,r,t) = \frac{\rho}{8\pi\sqrt{\pi}c^3}\exp\left(\frac{-r^2}{c^2 4t}\right)t^{-5/2}. \tag{D-2}$$

Taking the natural logarithm of both sides of equation D-2 gives

$$\begin{aligned}\ln(g(\rho,r,t)) &= \ln\left(\frac{\rho}{8\pi\sqrt{\pi}c^3}\right) - \frac{r^2}{c^2 4t} + \ln(t^{-5/2}) \\ &= \ln\left(\frac{\rho}{8\pi\sqrt{\pi}c^3}\right) - \frac{r^2}{c^2 4t} - \frac{5}{2}\ln(t).\end{aligned} \tag{D-3}$$

To find the time of the peak, differentiate equation D-3 with respect to t,

$$\frac{\partial[\ln(g(\rho,r,t))]}{\partial t} = \frac{r^2}{c^2 4t^2} - \frac{5}{2t}, \tag{D-4}$$

and set the result to zero, yielding

$$t_{\text{peak},r} = \frac{r^2}{10c^2} = \frac{\mu r^2}{10\rho}. \tag{D-6}$$

REFERENCES

Archie, G. E., 1942, The electrical resistivity log as an aid in determining some reservoir characteristics: Journal of Petroleum Technology, **5**, 1–8.
Constable, S. C., R. L. Parker, and C. G. Constable, 1987, Occam's inversion: A practical algorithm for generating smooth models from EM sounding data: Geophysics, **52**, 289–300.
Dahlin, T., and B. Zhou, 2004, A numerical comparison of 2D resistivity imaging with 10 electrode arrays: Geophysical Prospecting, **52**, 379–398.
Edwards, L. S., 1977, A modified pseudosection for resistivity and IP: Geophysics, **42**, 1020–1036.
Edwards, R. N., 1997, On the resource evaluation of marine gas hydrate deposits using sea-floor transient electric dipole-dipole methods: Geophysics, **62**, 63–74.
Kaufman, A. A., and G. V. Keller, 1983, Frequency and transient soundings: Elsevier Science Publ. Co., Inc.
Levinson, N., 1947, The Wiener rms (root mean square) error criterion in filter design and prediction: Journal of Mathematics and Physics, **25**, 261–278.
Loke, M. H., and R. D. Barker, 1996, Rapid least-squares inversion of apparent resistivity pseudo-sections using quasi-Newton method: Geophysical Prospecting, **48**, 152–181.
Newman, G. A., 1989, Deep transient electromagnetic soundings with a grounded source over near-surface conductors: Geophysical Journal, **98**, 587–601.
Parker, R. L., 1994, Linear problems with uncertain data, *in* Geophysical inverse theory: Princeton University Press, 119–198.
Robinson, E. A., 1957, Predictive decomposition of time series with applica-

tion to seismic exploration: Geophysics, **22**, 767–778.
———, 1967, Statistical communication and detection with special reference to digital data processing of radar and seismic signals: Charles Griffin.
Robinson, E. A., and O. A. Osman, 1996, Deconvolution 2: Geophysics Reprint Series: SEG.
Rocroi, J.-P., and F. Gole, 1983, Method of geophysical prospection using transient currents: U. S. Patent 4 417 210.
Spies, B. R., and D. E. Eggers, 1986, The use and mis-use of apparent resistivity in electromagnetic methods: Geophysics, **51**, 1462–1471.
Strack, K.-M., 1992, Exploration with deep transient electromagnetics: Elsevier Science Publ. Co., Inc.
Strack, K.-M., T. Hanstein, K. LeBrocq, D. C. Moss, K. Vozoff, and P. A. Wolfgram, 1989, Case histories of LOTEM surveys in hydrocarbon prospective areas: First Break, **7**, 467–477.
Webster, G. M., 1978, Deconvolution: Geophysics Reprints Series: SEG.
Weir, G., 1980, Transient electromagnetic fields about an infinitesimally long grounded horizontal electric dipole on the surface of a uniform half-space: Geophysical Journal of the Royal Astronomical Society, **61**, 41–56.
Wiener, N., 1949, Time series: Massachusetts Institute of Technology Press.
Wilson, A. J. S., 1997, The equivalent wavefield concept in multichannel transient electromagnetic surveying: Ph.D. thesis, University of Edinburgh.
Wright, D. A., 2003, Detection of hydrocarbons and their movement in a reservoir using time-lapse multi-transient electromagnetic (MTEM) data: Ph.D. thesis, University of Edinburgh.
Wright, D. A., A. Ziolkowski, and B. A. Hobbs, 2001, Hydrocarbon detection with a multichannel transient electromagnetic survey: 71st Annual International Meeting, SEG, Expanded Abstracts, 1435–1438.
———, 2002, Hydrocarbon detection and monitoring with a multichannel transient electromagnetic (MTEM) survey: The Leading Edge, **21**, 852–864.
———, 2005, Detection of subsurface resistivity contrasts with application to location of fluids: U. S. Patent 6 914 433.